Respiratory Research

RESEARCH

Open Access

TCF7 enhances pulmonary hypertension by boosting stressed natural killer cells and their interaction with pulmonary arterial smooth muscle cells

Li-Wei Wu[1,2,3†], Min Chen[4†], Dai-Ji Jiang[1,2,3†], Chen-Yu Jiang[1,2,3], Yi-Wei Liu[1,2,3], Bei Feng[1,2,3], Chen-Fei Shi[5], Xu Huang[1,2,3], Xu Zhang[1,2,3], Xiao-He Xu[6], Xing-Liang Zhou[1,2,3], Yi Shen[1,2,3], Tian-Yu Liu[1,2,3], Lin-Cai Ye[1,2,3], Yang-Yang He[5*†], Hao Zhang[1,2,3,4*†] and Yi Yan[1,2,3*†]

Abstract

Background Pulmonary hypertension (PH) is a life-threatening cardio-pulmonary disorder. Whether natural killer (NK) cells could act as participants in PH and the mechanism by which NK cells moderate pulmonary vascular remodeling has not been fully elucidated.

Methods Single-cell RNA sequencing data from lungs of human pulmonary arterial hypertension (PAH) patients and monocrotaline (MCT)-induced PH rat model were retrieved from GEO database or UCSC Cell Browser. Tcf7 conditional knockout mice and TCF7 overexpression following adeno-associated virus 6 (AAV6) intratracheal delivery in rats were generated. The NK92 cell line and primary human pulmonary artery smooth muscle cells (hPASMCs) were used for in vitro experiments.

Results Stressed NK cells were much higher in lungs from human PAH and MCT-induced PH compared to corresponding controls. Of note, TCF7 topped the list differentiating high-stressed from low-stressed human NK cells. TCF7-expressing NK cells displayed higher stress profile than TCF7-deficient cells. Tcf7-deficient NK cells exhibited lower Hsp90aa1 and Hsp90ab1 at transcriptional level and Hsp90 at protein level than Tcf7-expressing cells 24 h post-hypoxia. Mechanistically, TCF7-overexpressing NK cells secrete more SPP1 compared to control NK cells, thus promoting the proliferation and migration of hPASMCs 48 h post-hypoxia. TCF7 overexpression in rats aggravated PH features, while Tcf7 deficiency in mice alleviated pulmonary remodeling possibly due to the manipulation of HSP90 level in NK cells and SPP1 in the microenvironment.

†Li-Wei Wu, Min Chen and Dai-Ji Jiang contributed equally to this work and shared first authorship.

†Yang-Yang He, Hao Zhang and Yi Yan contributed equally to this work and shared last authorship.

*Correspondence:
Yang-Yang He
heyangyang@vip.henu.edu.cn
Hao Zhang
drzhanghao@126.com
Yi Yan
yannie0928@163.com
Full list of author information is available at the end of the article

Conclusions TCF7 contributes to the immunopathology of PH possibly through upregulation of stressed NK cells. Under stress conditions, NK cells promote the proliferation and migration of hPASMC through paracrine effects, thereby further promoting vascular remodeling.

Keywords Pulmonary hypertension, Single cell RNA-seq, Natural killer cells, TCF7, Pulmonary arterial smooth muscle cells

Introduction

Pulmonary hypertension (PH) is a progressive and life-threatening cardio-pulmonary disorder characterized by elevated pulmonary vascular resistance (Mean Pulmonary Artery Pressure (mPAP) >20 mmHg), leading to right ventricular failure and ultimately, if left untreated, to death [1, 2]. Pulmonary arterial hypertension (PAH) is a subtype of PH, referring to group 1 PH, mainly including idiopathic PAH, heritable PAH, drug- and toxin-associated PAH, disease-associated (connective tissue disease, HIV infection, portal hypertension, congenital heart disease and schistosomiasis) PAH, PAH with features of venous/capillary involvement, and persistent PH of the newborn. The etiology of PH is multifactorial and complex, involving the interplay of genetic, epigenetic, metabolic, and immunological factors that contribute to aberrant pulmonary vascular remodeling [3–5]. The current treatments for PH are mostly focused on vasodilation, and there are still no effective interventions for the immune microenvironment around the pulmonary vasculature [6].

Natural killer (NK) cells, as essential effectors of the innate immune system, are known to play a pivotal role in the regulation of immune responses, exerting functions ranging from cytotoxicity to the secretion of immunomodulatory cytokines [7–9]. Zeming Zhang et al. points out that NK cells exhibit a stress response driven by chronic hypoxia in tumors, and this phenotype weakens the function of NK cells, which in turn makes it easier for the tumors to achieve immune evasion [10]. Chronic hypoxia is also attributable to PH progression [11]. However, the contributions of NK cellular stress response to the pathogenesis of PH and their potential as therapeutic targets remain unclear. The specific interactions between NK cells and pulmonary arterial smooth muscle cells (PASMCs) have not yet been fully revealed as well. A comprehensive single-cell RNA sequencing analysis of lung tissues from both human and experimental models of PH would be able to figure out novel mediators of NK cells driving PH development. This aids in the nuanced understanding of the disease's immunopathology, particularly regarding the contribution of NK subsets within the lung microenvironment.

Transcription factor 7 (TCF7), a member of the T-cell factor/lymphoid enhancer factor (TCF/LEF) family, is primarily recognized for its role in T-cell development and differentiation [12, 13]. Several studies also suggested that TCF7 may extend its influence beyond the adaptive immune system to innate immune cells such as NK cells [14–16]. In graft-versus-host disease, there exists a unique subset of $TCF7^{high}$ NK cells, which suppress the function of CD4-positive T cells [15]. In tumors, NK cells with reduced expression levels of TCF7 exhibit stronger cytotoxic killing effects [17]. Additionally, TCF7 plays an important role in the development and maturation of NK cells, and immature NK cells with TCF7 deficiency are unable to develop and mature properly, resulting in significant functional deficiencies [18]. Nevertheless, the functional and molecular determinants of TCF7 in NK cell fate in the context of PH have been poorly characterized.

Hence, our study aims to explore the transcriptional landscape of NK cells and whether NK cell behavior could be regulated by TCF7 utilizing single-cell RNA sequencing data from both human PAH and rodent PH models. We seek to decode the complexity of NK cell dynamics, uncover the transcriptional underpinnings that dictate the NK cell stress response and elucidate their interaction with PASMCs driving PH.

Methods

Single-cell RNA sequencing data processing

We sourced single-cell RNA sequencing data of lung tissues from human PAH from the Gene Expression Omnibus (GEO) repository (https://www.ncbi.nlm.nih.gov/geo/), under accession number GSE228644 [19]. The dataset encompassed samples from three healthy donors and three patients diagnosed with PAH. For each individual sample, we transformed the raw gene expression matrix into a Seurat object utilizing the Seurat R package (v5.0.1) in conjunction with the R software (v4.2.3) [20]. Rigorous quality control measures entailed the exclusion of cells that fell below the thresholds of 1000 unique molecular identifiers (UMIs), 500 detected genes, or exhibited mitochondrial gene content exceeding 15%. Similarly, genes present in fewer than 10 cells were deemed infrequently expressed and therefore omitted by the data provider. The resulting dataset underwent logarithmic normalization via the NormalizeData

function and was subsequently scaled using the ScaleData function, accounting for variability in UMI counts and mitochondrial gene proportions. We merged the gene expression matrices from all samples, and neutralized batch effects using Seurat's FindIntegrationAnchors and IntegrateData functions. Dimensionality reduction was executed utilizing the RunUMAP function, retaining the foremost 20 dimensions, and cellular clustering was achieved through the FindClusters function at a resolution of 0.8, maintaining all default settings otherwise. Marker genes for each cluster were pinpointed using the FindAllMarkers function. We validated cell types against the CellMarker database (http://xteam.xbio.top/CellMarker/), supplemented by manual annotation for accuracy [21].

The same procedure, including normalization, scaling, dimensionality reduction, and cellular clustering and annotation, was repeated for monocrotaline (MCT) induced PH rat model at single-cell RNA level, and the datasets consisting of lung tissues from six wild-type and six MCT-induced PH rats were obtained from the UCSC Cell Browser (http://mergeomics.research.idre.ucla.edu/PVDSingleCell/CellBrowser/) [22]. Moreover, we extracted and isolated NK cells from each dataset and reiterated the mentioned processes.

Calculation of NK functionality scores

To gauge the NK cell activity, we computed NK functionality scores for each NK cell via the AddModuleScore function in Seurat. We leveraged predefined gene sets relating to NK functions (refer to Table S1 in the Supporting Information). NK cells were then stratified based on stress score into low- and high stress groups. Using the FindAllMarkers function, we identified significant differentially expressed genes (average log fold change > 0.25, $p < 0.05$) between two groups.

Functional enrichment analysis

The Metascape database (https://metascape.org/gp/) [23] provided a platform for further enrichment investigation within biological processes as identified by Gene Ontology (GO), by selecting genes exhibiting differential expression beyond a threshold of log fold change > 0.25 and adjusted p-value < 0.05.

Cell communication analysis

Cellchat R package was uesd to analyze the strength and relationships of communication between cells. The Cellchat analysis object was created using a Seurat object and human database was set up as the reference data for receptor-ligand pairs. Finally, we used the reference data to calculate the strength of communication between cells and obtain the expression differences of various receptor-ligand pairs. Visualization was performed using the visualization commands provided with the Cellchat package.

Patient lung tissue acquisition

The lung tissue was donated by deceased patients. After harvest of the lung tissues, they were cut into small pieces and stored in a freezer at −80℃. This study has been approved by the Ethics Committee of Shanghai Children's Medical Center affiliated to Shanghai Jiao Tong University School of Medicine (SCMCIRB-K2024081-1), and informed consent has been obtained from the patients or their relative guardians.

Animals

To explore the role of TCF7 in the development of PH, CAGGCre-ERTM; $Tcf7^{flox/flox}$ mice ($Tcf7^{KO}$) mice were generated by interbreeding C57BL/6 J $Tcf7^{flox/flox}$ mice with CAGGCre-ERTM mice. To invoke Tcf7 gene knockout, mice received a 5-day regimen of 75 mg/kg tamoxifen (dissolved in corn oil at 20 mg/ml). These mouse strains were acquired from Cyagen Biosciences Inc. $Tcf7^{KO}$ male mice (8-week, 20 g) or their wild-type littermates $Tcf7^{flox/flox}$ mice ($Tcf7^{WT}$) were either housed in hypoxic chamber (Shanghai TOW Intelligent Technology Co., Ltd, ProOX-850) (10% O_2) or at ambient air for four weeks.

To explore whether up-regulation of TCF7 could exacerbate disease progression, human TCF7 was engineered and packaged into adeno-associated virus 6 (AAV6). Male Sprague-Dawley rats were obtained from Beijing Vital River Laboratory Animal Technology Co., Ltd., and received intratracheal delivery of 100μl of either AAV6-hTCF7 or AAV6 vector at a dosage of 4×10^{12} GC/ml, followed by intraperitoneal MCT administration (Sigma, Cat #C2401; 60 mg/kg) or saline injection. The hypoxia rats were housed in hypoxic chamber (Shanghai TOW Intelligent Technology Co., Ltd, ProOX-850) (10% O_2) for three weeks.

All rodents were housed under specific pathogen-free conditions and organs were harvested at week 3 for rat models and week 4 for murine models after right heart catheterization. The degree of right ventricular hypertrophy was determined via the Fulton index, which equals to the ratio of the weight of right ventricle (RV) to the total mass of the left ventricle (LV) and the interventricular septum.

The experiment was carried out in accordance with the Guideline for Care and Use of Laboratory Animals published by the US National Institutes of Health and the Guidelines for the ethical review of laboratory animal welfare People's Republic of China National Standard GB/T 35892-2018 [24]. All the protocols and procedures

were approved by the Animal Ethics Committee of Shanghai Children's Medical Center, Shanghai Jiao Tong University School of Medicine.

Right heart catheterization

Invasive hemodynamic measurements were obtained through right ventricular catheterization with a Millar pressure catheter (SPR-671; Millar Inc.) in mice, and via jugular vein cannulation in rats using a PE50 catheter. The mice (200 mg/kg) and rats (125 mg/kg) were both anesthetized with tribromoethanol. Data were recorded, analog-to-digital converted (PowerLab; AD Instruments) and analyzed using LabChart software (AD Instruments, v8.1.16).

Vascular remodeling analysis

We quantified the extent of pulmonary arteriolar remodeling by comparing the thickness of the vascular media wall to the external diameter of distal pulmonary arterioles (50–100 μm) on lung sections stained with Elastica van Gieson (EVG). Collagen deposition within the arterioles was assessed by Masson's trichrome staining. Muscularization was evaluated based on the proportion of α-smooth muscle actin (α-SMA)-positive cells enveloping the vessel, stratified as non-muscularized, partially muscularized, or fully muscularized. At least 30 appropriately size-matched vessels in non-sequential lung sections of each animal were analyzed.

Immunostaining assay

Following deparaffinization, rehydration, endogenous peroxidase activity inhibition, and antigen retrieval, paraffin-embedded tissue blocks were sectioned into 5-μm slices for staining. The sections underwent permeabilization with 0.1% Triton X-100 (Sigma-Aldrich; Cat #T8787) in phosphate-buffered saline (PBS) and were then incubated with primary antibodies overnight at 4 °C. This was followed by incubation with the corresponding secondary antibodies. The primary antibodies were anti-vWF (Invitrogen, Cat #PA5-104687), anti-α-SMA (Servicebio, Cat #GB12044-100), anti-HSP90 (Invitrogen, Cat #MA5-33168), anti-NK1.1 (Invitrogen, Cat #MA1-70100). The TSA reagent kits (ABclonal, Cat #RK05903) were used for fluorescence labeling, with emission wavelengths corresponding to 520 nm (green), 570 nm (red), and 690 nm (pink). Cell nuclei were counterstained using 4′,6-diamidino-2-phenylindole (DAPI; Sigma-Aldrich; Cat #D9542). Detailed morphological examination was facilitated by imaging with a laser scanning confocal microscope (LSM880; Zeiss, Germany).

Cell culture and reagents

The primary mouse NK cells were obtained from $Tcf7^{KO}$ and $Tcf7^{WT}$ mice with mouse NK cell isolation kit (Biolegend, Cat #480050). 1×10^8 NK cells were seeded into plate/dish and cultured in RPMI 1640 medium supplemented with 10%fetal bovine serum (FBS), 10% Horse Serum (Gibco), and recombinant mouse IL-2 (abcam, Cat #ab259380). The NK92 cell line was obtained from QuiCell Biotech Company. 1×10^6 NK92 cells were seeded into plate/dish and cultured in MEMα medium supplemented with 20% FBS, 0.2 mM Inositol, 0.1 mM β-mercaptoethanol, 0.02 mM folic acid, and recombinant human IL-2 (abcam, Cat #ab119439).

The primary human PASMCs (hPASMCs) were isolated from pulmonary bulla patient lung tissues. In brief, pulmonary arteries from pulmonary bulla patient lung tissues were isolated under a dissecting microscope. The adventitia was removed with fine micro-scissors and endothelial layer were removed with cell scraper. Next, minced arteries were attached to bottom of cell culture dish and then immersed by DMEM/F12 containing 20% FBS, 100 U/mL penicillin and 100 μg/mL streptomycin in a 37 °C, 5% CO_2 humidified incubator. Five days later, culture media were refreshed, and non-adherent cells were removed. Ten days later the adherent cells that had grown to 90% confluence were considered as passage 0. The isolated hPASMCs were cultured in DMEM/F12 medium supplemented with 10% FBS and passage 4–6 were used for subsequent experiments. The NK92 cells were either cultured in normoxia condition at 37 °C in the cell incubator or in hypoxia chamber (Don Whitley Scientific Limited, Model: H35) for 48 h at 37 °C with 1%O_2 and 5% CO_2.

Lentiviral infection

We infected the NK92 cell line using a TCF7 overexpression lentivirus (LV-TCF7) or control lentivirus (LV-Con) at a multiplicity of infection (MOI) of 20. After centrifugation of the cells and removal of most of the supernatant, the calculated volume of viral solution was added to the 15 mL tube and incubated at room temperature for 15 min. Subsequently, sufficient culture medium was added to the cells, which were then seeded into a 6-well plate, with each well containing 1×10^6 NK92 cells.

Cell viability and proliferation

NK92 cells were infected with TCF7 overexpression lentivirus or control lentivirus as aforementioned for 72 h. Next NK92 cells were cultured in the incubator or hypoxia chamber for 48 h. hPASMCs were seeded into a 96-well plate (0.8×10^5/mL) 24 h before starvation (DMEM/F12 without FBS for 24 h). The supernatant from TCF7 overexpression- or control lentivirus infected NK92 cells were added into hPASMC for another 24 h. To assess cell viability, cell supernatants were discarded and replaced with CCK8 solution (Dojindo Molecular

Technologies Inc, Kumamoto, Japan), cells were then incubated at 37 °C with 5% CO2 for 1 h. Optical density (OD) was determined at 450 nm using a microplate reader (Infinite M200 Pro; Tecan, Switzerland). To examine cell proliferation, EdU assay was performed according to the manufacturer's instructions (Servicebio, Cat #G1603). After cellular EdU labeling, fixation and permeabilization, cells were washed with PBS buffer followed by EdU click reaction. After 2–3 times wash with PBS buffer, cells were incubated with diluted Hoechst 33342 staining solution (1:1000 dilution) for 5 min. Next, the solution was removed and cells were washed with PBS buffer twice. Lastly, images were taken using a fluorescence microscope.

Transwell assay

hPASMCs were starved (DMEM/F12 without FBS) for 24 h. DMEM/F12 medium and supernatants from either TCF7 overexpression lentivirus or control lentivirus infected NK92 cells after hypoxia challenge for 48 h at a ratio of 1:1 were collected. hPASMCs were then resuspended with the mixture at a density of 1×10^6/mL. DMEM/F12 medium containing 20% FBS was added to the lower chamber of a 24-well plate. Subsequently, 100 µL cell suspension were added into upper chamber and cultured at the incubator for 24 h. The transwell insert was removed, the culture medium was discarded, and the cells at the insert bottom were fixed with 4% paraformaldehyde for 30 min followed by PBS buffer wash twice. Next, the cells were stained with crystal violet (Keygen-Biotech, Cat #KGA229) for 30 min and the insert were washed with running water twice gently. Finally, images were taken using a microscope for documentation after air-drying of the insert for 24 h.

Flow cytometry

Dissociated lung, spleen, and blood samples were first processed into single-cell suspensions. Subsequently, cells were incubated with the following antibodies at 4°C: anti-CD45-APC-CY7 (Invitrogen, Cat #A15395), anti-CD3-PerCP (Invitrogen; Cat #45-0031−82), and anti-NK1.1-APC (Invitrogen; Cat #17–5941−82). After fixation and permeabilization, Cells were further stained with anti-HSP90 (Invitrogen, Cat #MA5-33168) antibody followed by the secondary goat anti-rabbit IgG-FITC (Invitrogen; Cat #F-2765) antibody, and analyzed on a Beckman CytoFLEX flow cytometer.

Quantitative real-time polymerase chain reaction (qRT-PCR)

We extracted total RNA using the RNAeasy™ Animal RNA Isolation Kit with Spin Column (Beyotime, Cat #R0026). Reverse transcription was performed utilizing HiScript II Q RT SuperMix for qPCR (+gDNA wiper) (Vazyme, Cat #R223-01), per the manufacturer's instructions. Quantitative real-time PCR (qRT-PCR) was employed to quantify gene transcription levels using ChamQ Universal SYBR qPCR Master Mix (Vazyme, Cat #Q711-02) along with respective primer pairs (see Table S2 in the Supporting Information). We examined mRNA expression for each gene in three technical replicates.

Western blot

Cells and tissues were lysed in RIPA buffer (Beyotime, Cat #P0013B) to extract total protein. The total protein was quantified, and equal amounts of protein were separated by sodium dodecyl sulfate–polyacrylamide gel electrophoresis (SDS–PAGE), followed by transfer onto nitrocellulose membranes. The membranes were incubated overnight at 4°C with primary antibodies: anti-SPP1 (Invitrogen, Cat #PA5-34579), anti-TCF7 (CST, Cat #2203), and anti-GAPDH (CST, Cat #2118). This was followed by a two-hour incubation at room temperature with goat anti-rabbit HRP-conjugated secondary antibody (Beyotime, Cat #A0208). Immunodetection was accomplished using an enhanced chemiluminescence detection system.

Statistical analysis

Statistical analyses were implemented in R (v4.2.3) or Graphpad prism (v9.5.1) as specified in the figure legends. Kolmogorov-Smirnov test was used to confirm normality of data distribution. The comparison between two groups was determined using two-tailed Student's *t*-test if the data were normally distributed, and Wilcoxon rank-sum test was used if otherwise. One-way ANOVA was applied to compare the difference among three groups or above if data were normally distributed, and Kruskal-Wallis test was adopted if not normally distributed. A *P*-value of less than 0.05 indicated significance.

Results

NK cell atlas in lung tissues from PAH patients and controls

In this study, a total of 20,035 cells from 3 normal and 3 PAH lung tissue samples were classified into 15 principal cell types (Fig. 1A and Figure S1 A), with the principal marker genes for each cell type displayed in Figure S1B. An appreciable degree of heterogeneity was observed in cells derived from both normal lung tissues and those affected by PAH (Fig. 1B), indicating significant alterations in the microenvironment within the PAH lung compartments. It was reported NK cells exhibited a phenotypic transformation characterized by reduced cytotoxicity in PAH [8]. However, other phenotypes of NK cells in this disease setting have not been fully explored.

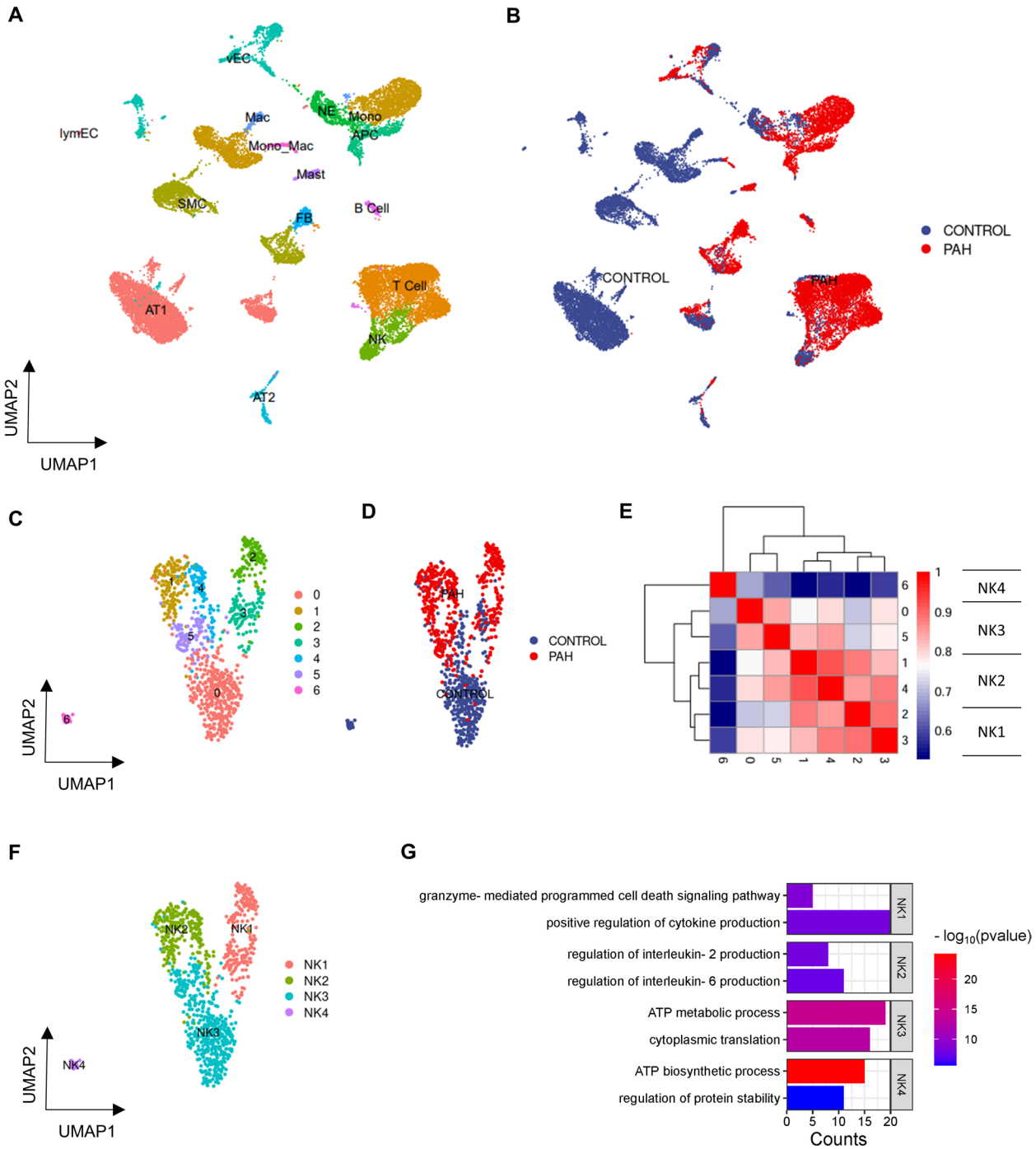

Fig. 1 The NK landscape of lung tissues from PAH patients and controls at single-cell resolution. **A** All cells in lung tissues from three PAH patients and three controls were clustered into 15 major cell types and visualized in UMAP plot. Each dot represents a cell, colored by cell type. **B** Cell distributions in lung tissues from either PAH patients or controls and were visualized in UMAP plot. **C** NK cells categorized into seven subclusters. **D** Distribution of lung NK cells from either PAH patients or controls. **E** Correlation between NK cells subsets and was visualized in heatmap. Red represents high correlation while blue represents low correlation. **F** NK cells clustered into four NK functional subtypes based on correlation. **G** Enriched GO biological process among different NK subtypes. Red bar represents lower *P*-value while blue bar represents higher *P*-value

A total of 952 NK cells were grouped into 7 distinct subpopulations (Fig. 1C). Upon analysis, NK cells derived from different groups showed considerable heterogeneity split by their origin (Fig. 1D). Correlation analysis utilizing representative genes of NK cells revealed that these 7 NK cell subgroups could be subdivided into 4 major functional subsets (Fig. 1E, F). The top 10 marker genes of 4 major functional subsets were shown in Table S3. Pathway enrichment of marker genes for these four subsets showed that NK1 cells were primarily responsible for cytokine secretion and exerted cytotoxic functions; NK2 cells were mainly involved in the secretion of IL2 and IL6; NK3 cells partook in ATP metabolism and cytoskeletal transportation, while NK4 cells engaged in ATP synthesis and regulation of protein stability (Fig. 1G).

NK cell landscape in lung tissues from MCT-induced PH rats and controls

A total of 22,161 cells from the lung tissues of 6 control and 6 MCT-induced PH rats were classified into 16 major cell types (Fig. 2A and Figure S2 A) and visualized by group (Fig. 2B). To annotate the cell types, top 3 marker genes were displayed in Figure S2B. Of these, 2,063 NK cells were subdivided into 4 distinct subpopulations (Fig. 2C). In contrast to human data, there was no remarkable heterogeneity between lung NK cells from MCT-PH rats versus those from controls (Fig. 2D). Based on the correlation analysis of characteristic genes, NK cells were further divided into 3 functional subsets (Fig. 2E, F). The top 10 marker genes of 3 functional subsets were shown in Table S3. These functional subsets exhibited different roles: NK1 predominantly engaged in cell adhesion and apoptotic pathways, NK2 was primarily involved in the NF-kappaB signaling and programmed cell death, while NK3 was mainly responsible for cell activation and perforin-mediated cytotoxicity (Fig. 2G).

Heightened stressed NK cells in PH lungs and TCF7 affects NK functionality

In the tumor, the stress response of NK cells is activated by chronic hypoxia, leading to impaired NK cell function, which in turn makes the tumor cells in tumor microenvironment more prone to immune escape [10]. In similarity to cancer, a state of chronic hypoxia also triggers the development of PH. Therefore, stress score for each NK cell was calculated based on the expression of stress-related genes [10]. NK cells from PAH group exhibited higher stress scores compared to that of controls (Fig. 3A), suggesting a phenotypic transformation of NK cells in favor of stress response in microenvironment of PAH. This is also evidenced by a significant decrease in cell cytotoxicity (Figure S3 A) and little change was detected in inflammatory response (Figure S3B). Cell cytotoxicity and the secretion of inflammatory cytokines are also important phenotypes of NK cells [10, 25]. The enhanced stress response of NK cells under hypoxic conditions may impact cytotoxicity. A much higher stress score was observed in both NK1 and NK2 compared to that of NK3 or NK4 (Fig. 3B), further implicating a relevant link between NK1/2 and the progression of pulmonary vascular remodeling. Next, we divided the NK cells according to the median stress score, it turned out that TCF7 topped the differentially expressed genes and was much higher in high- versus low-stressed NK cells (Fig. 3C). Compared to $TCF7^{-}$ NK cells, $TCF7^{+}$ NK cells displayed higher stress score (Fig. 3D) and lower cytotoxicity score (Figure S3 C). The findings in human lung tissue, the stress response of NK cells was elevated in the MCT treated group (Fig. 3G), while cytotoxicity was decreased (Figure S4 A), and no significant difference in inflammatory response was observed between the two groups (Figure S4B). The stress scores of the NK cell functional subgroups NK2 and NK3 were elevated (Fig. 3H). There was an increased trend of stress score in Tcf7-exthat of controls (Fig. 3E, Figure S3E, F), as well as in lung NK1 and NK2 from PH patients (Fig. 3F). This suggests that NK1 and NK2 cells with high expression of TCF7 might be a type of NK cells responded to stress.

Consistent with findings in human lung tissue, the stress response of NK cells was elevated in the MCT treated group (Fig. 3G), while cytotoxicity was decreased (Figure S4 A), and no significant difference in inflammatory response was observed between the two groups (Figure S4B). The stress scores of the NK cell functional subgroups NK2 and NK3 were elevated (Fig. 3H). There was an increased trend of stress score in Tcf7-expressing rat NK cells compared to that of Tcf7-deficient rat NK cells although it didn't reach statistical significance (Fig. 3I). Cytotoxicity scores were markedly decreased in Tcf7-positive NK cells (Figure S4 C), while the scores of inflammatory responses did not differ between the groups (Figure S4D). Tcf7 was much higher in lung tissues from MCT-induced PH rats compared to that of controls at both mRNA and protein levels (Fig. 3J, K, Figure S4E, F), as well as in lung NK2/3 subtypes from rodent PH model at single-cell level (Fig. 3L).

TCF7 regulates the stress response of NK cells

A total of 23 stress-related genes were upregulated in human PAH group (Fig. 4A), and 19 stress-related genes were upregulated in the TCF7-expressing NK cells (Fig. 4B). Of note, the expression levels of several heat shock-related proteins were elevated, so we selected the four genes with high expression levels for further validation. NK cells were harvested from the spleens of Tcf7 knockout mice and their controls. Tcf7

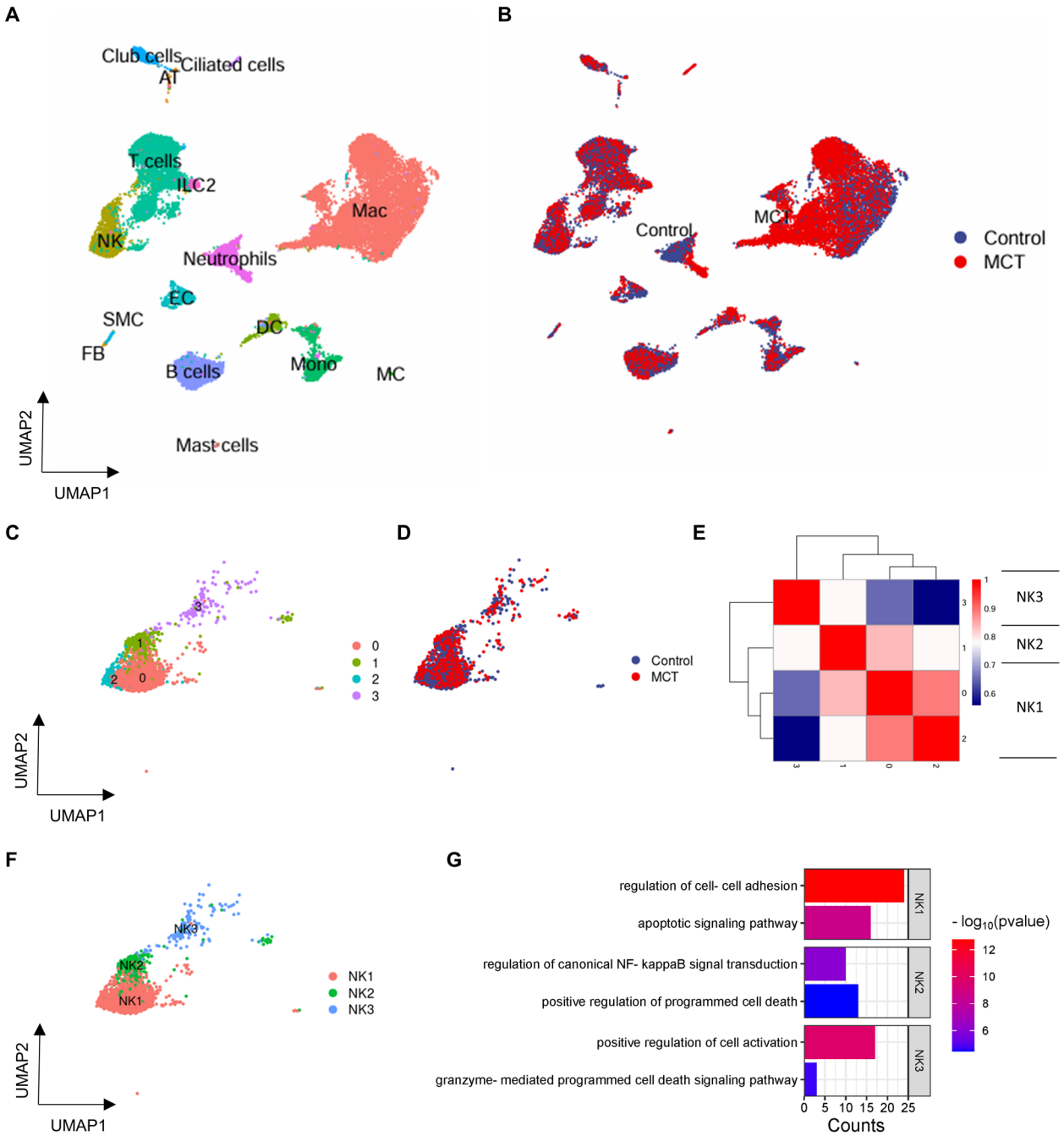

Fig. 2 The NK landscape of lung tissues from MCT-induced PH rat model and controls at single-cell resolution. **A** All cells in lung tissues from six MCT-induced PH rats and six controls clustered into 16 major cell types and were visualized in UMAP plot. Each dot represents a cell, colored by cell type. **B** Cell distributions in lung tissues from either MCT-induced PH rats or controls. **C** NK cells clustered into four clusters. **D** Distribution of lung NK cells from either MCT-PH rats or controls. **E** Correlation between NK cells subsets and was visualized in heatmap. Red represents high correlation while blue represents low correlation. **F** NK cells clustered into three NK subtypes based on correlation. **G** GO biological process shows functional enrichment among NK subtypes. Red bar represents lower *P*-value while blue bar represents higher *P*-value

deficiency was evidenced by ~75% reduction at protein level in TCF^{KO} NK cells (Fig. 4C, D). The in vitro experimental schematic for gene validation was shown in Fig. 4E. Both *Hsp90aa1* and *Hsp90ab1* were much higher in $Tcf7^{WT}$ NK cells compared to those in $Tcf7^{KO}$ NK cells (Fig. 4F, G and Figure S5 A, B), whereas no significant difference was observed for *Hsph1* and *Hsp90b1* between the two groups (Figure S5 C, D).

Consistently, stress-related genes were also found to be upregulated in rat NK cell functional subsets NK1 and NK2 at single-cell level (Figure S5E). Moreover, a downregulation of HSP90 was demonstrated from $Tcf7^{KO}$ NK cells compared to $Tcf7^{WT}$ NK cells after 24 h hypoxia (Fig. 4H). In line with the in vitro data, downregulation of HSP90 was also detected in lung NK cells from $Tcf7^{KO}$ mice (Fig. 4I). However, no significant difference was observed in HSP90 at protein level in blood or spleen between NK cells from $Tcf7^{KO}$ mice and those from $Tcf7^{WT}$ mice after 4-week hypoxia (Figure S6 A, B). These findings indicate that TCF7 may regulate the stress response of NK cells via the regulation of HSP90 expression in lung microenvironment.

TCF7 enhances proliferation and migration of PASMCs via upregulating secretion of SPP1 by NK cells

There were more signals from NK cells to PASMCs in the lung tissues from PAH compared that of controls (Fig. 5A). Of note, TCF7-expressing NK cells exhibit markedly increased SPP1-integrin interactions with PASMCs compared to TCF7-deficient counterparts in PH (Fig. 5B), suggesting that TCF7 might have an influence on the cell communication between NK cells and PASMCs through SPP1-mediated engagement with integrin receptors, potentially altering PASMC phenotype. To test the hypothesis, NK92 cells were infected by either TCF7 overexpression lentivirus (LV-TCF7) or control lentivirus (LV-Con) followed by hypoxia exposure. The hypoxic level was validated by *HIF1 A* mRNA expression level (Figure S7 A-C). It was shown that LV-TCF7 infected NK92 cells had a higher expression of SPP1 at protein level compared to LV-Con infected NK92 cells (Fig. 5C). It was observed that hPASMCs exhibited an increase in cell viability and proliferation rate after treatment with supernatant from LV-TCF7 infected NK92 cells compared to those treated with supernatant from LV-Con infected NK92 cells (Fig. 5D, E). Moreover, there was a 2.5-fold higher migratory capacity of hPASMCs treated with supernatant from LV-TCF7 infected NK92 cells as well (Fig. 5F).

TCF7 overexpression aggregates vascular remodeling in MCT-PH model

We next investigated the role of TCF7 in PH development. The experimental schematic was illustrated in Fig. 6A. After intratracheal delivery, a ~10-fold increase of TCF7 expression was observed in lungs from AAV6-hTCF7 rats at transcriptional level in Figure S8 A and S8B. The susceptibility of AAV6-hTCF7 rats to the MCT challenge (60 mg/kg) was then determined. AAV6-hTCF7 rats displayed significantly higher right ventricular systolic pressure (Fig. 6B), mean pulmonary arterial pressure (Fig. 6C), and Fulton index (Fig. 6D) compared to AAV6-Control treated rats 3 weeks after MCT administration. Additionally, TCF7 facilitated pulmonary arterial remodeling, resulting in thickening of the pulmonary artery medial layer (Fig. 6E, F) and more abundant deposition of collagen around the vessels (Fig. 6G, H), and more severe pulmonary vascular muscularization evidenced by a higher proportion of fully-muscularized vessels (Fig. 6I, J) compared to AAV6-Control rats at week 3 post MCT induction. Moreover, there was a higher proportion of $HSP90^{+}$ NK cells in lungs from MCT-treated PH rats receiving AAV6-hTCF7 compared to that of AAV6-Control recipients after MCT administration (Fig. 6K, L). There were also increased expression of SPP1 and TCF7 at protein level in lungs from rats receiving AAV6-hTCF7 compared to that of AAV6-Control recipients after MCT administration (Fig. 6M, N, O).

TCF7 overexpression aggregates vascular remodeling in hypoxia-PH model

AAV6-hTCF7 rats displayed significantly higher right ventricular systolic pressure (Figure S9 A), mean pulmonary arterial pressure (Figure S9B), and Fulton index (Figure S9 C) compared to AAV6-Control treated rats 3 weeks after hypoxia exposure. Similarly, TCF7 also exacerbated pulmonary vascular remodeling, as manifested by thicker pulmonary artery medial layer (Figure S9D, E) and more abundant deposition of collagen (Figure S9

(See figure on next page.)

Fig. 3 The association of TCF7 and stress response in NK cells. **A** Stress score of lung NK cells from controls or PAH patients (n=3 each). **B** Stress score of each human NK cell subtypes in lung tissues. **C** Top 10 stress related genes differentiating low- and high-stress NK cells; red represents high expression while blue represents low expression. **D** Stress score of TCF7-deficient or TCF7-expressing NK cells. **E** Lung *TCF7* expression level from controls or PAH patients (n=3 each). **F** *TCF7* expression level of four NK cell subclusters from controls or PAH patients. Blue indicates elevated expression levels, and gray indicates reduced or absent expression. **G** Stress score of lung NK cells from control or MCT-PH rats (n=6 each). **H** Stress score of each rat NK cell subtypes in lung tissues. **I** Stress score of Tcf7-deficient or Tcf7-expressing NK cells. **J** Lung *Tcf7* transcriptional levels from control group and MCT-PH group. **K** Lung Tcf7 protein levels from control group and MCT-PH group. **L** Lung *Tcf7* expression level of three NK cell subclusters from control or MCT-PH rats. Data represent mean ± SEM. * $P < 0.05$ compared to corresponding controls, as analyzed by unpaired t test or Mann-Whitney test as appropriate. Kruskal-Wallis was performed for the comparison among three groups or above

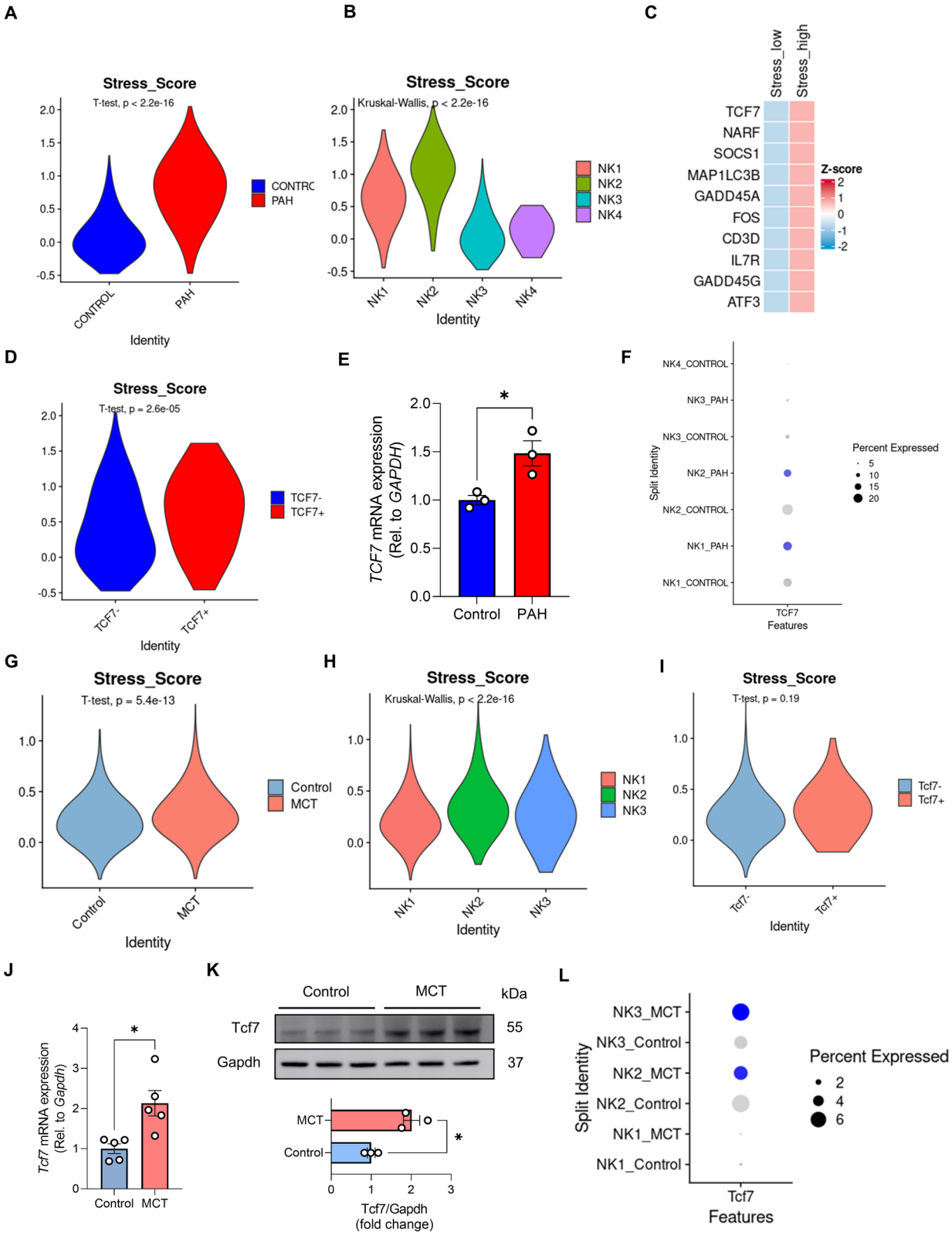

Fig. 3 (See legend on previous page.)

F, G), and higher proportion of fully-muscularized vessels (Figure S9H, I) compared to AAV6-Control recipients at week 3 post hypoxia challenge. Additionally, a higher proportion of $HSP90^+$ NK cells was also observed in lungs from hypoxia-induced PH rats receiving AAV6-hTCF7 administration (Figure S9 J, K). Rats receiving AAV6-hTCF7 displayed higher protein levels of SPP1 and TCF7 in lungs compared to that of AAV6-Control recipients after hypoxia exposure (Figure S9L, M, N).

TCF7 deficiency ameliorates vascular remodeling in murine PH model induced by hypoxia

The experimental design is illustrated in Fig. 7A. After intraperitoneal injection of tamoxifen, a robust decrease in Tcf7 expression was observed in lungs from Tcf7 knock out mice in Figure S10. $Tcf7^{KO}$ mice had improved hemodynamic compromise and right ventricular hypertrophy evidenced by lower RVSP and Fulton index compared to those in $Tcf7^{WT}$ mice at day 28 post-hypoxia (Fig. 7B, C). In contrast to the overexpression experiment, TCF7 knockout ameliorated pulmonary artery remodeling under hypoxic conditions, resulting in the thinning of the medial layer (Fig. 7D, E) and reduced perivascular collagen deposition (Fig. 7F, G), as well as less proportion of fully muscularized vessels (Fig. 7H, I). Additionally, TCF7 knockout resulted in a decreased proportion of NK cells expressing HSP90 (Fig. 7J, K). TCF7 knockout resulted in decreased SPP1 and TCF7 expression at protein levels in mouse lung tissues (Fig. 7L, M, N). All the findings implicate that TCF7 deficiency might contribute to a less stress levels of NK cells and less SPP1 protein levels at the microenvironment in PH.

Discussion

In this study, we advanced the comprehensive understanding of the complexities of NK cells and their crosstalk with PASMCs. By combining single-cell RNA sequencing data from both human PAH and MCT-induced PH model with functional assessments, we have provided evidence that suggests altered behavior of NK cells in the context of PH in both humans and rodents. This alteration in cellular behavior may be attributable to the differential expression patterns of TCF7. Overexpression of TCF7 exacerbated key features of PH, including vascular remodeling and right ventricular hypertrophy in MCT-induced PH model. Conversely, TCF7-deficient mice exhibited improved pulmonary hemodynamics and vascular pathology after hypoxia exposure. This improvement may be attributable to the altered behavior of stressed NK cells, particularly through their secretion of SPP1, which appears to regulate the proliferation and migration of PASMCs. Our findings provide compelling evidence that TCF7 contributes to PH pathogenesis and suggest that it may serve as a therapeutic target for the disease.

Among the various components of innate immunity, the roles of macrophages have been widely explored; however, the understanding of NK cell function in relation to PH remains limited. The phenotype of NK cells characterized by reduced cytotoxicity in PH was depicted in our results. In line with our study, the cytotoxicity of NK cells has been found to be downregulated in patients with PAH [8]. By contrast, there was an increase in the stress score in PH NK cells compared to that of the control group, supporting a state of heightened stress response. The abnormal NK cell stress response has been previously reported in cancers. In the hostile tumor microenvironment, elevated levels of reactive oxygen species (ROS) impair the function of NK cells. ROS are associated with cellular stress responses, primarily through the inhibition of the transcription factor NRF2, thereby heightening the stress responses in cells and consequently damaging their function. Targeted activation of NRF2 has the potential to reverse the enhanced cellular stress responses caused by increased ROS, thereby restoring the functionality of NK cells [26]. Our findings implicate that NK cells in PH may face similar functional shifts impacting their cytotoxic capabilities.

(See figure on next page.)

Fig. 4 TCF7 might act as a moderator of NK cells responded to stress. **A** The expression of stress-related genes of lung NK cells from PAH patients or controls. Circle sizes represent the proportions of cells expressing genes of interest and filled colors from light gray to blue represent normalized expression levels from low to high. **B** The expression of stress-related genes of human lung $TCF7^-$ or $TCF7^+$ NK cells. **C** Representative histogram of flow cytometry showing Tcf7 expression of isolated spleen NK cells from $Tcf7^{WT}$ or $Tcf7^{KO}$ mice. **D** Proportion of $Tcf7^+$ NK cells among all NK cells from $Tcf7^{WT}$ or $Tcf7^{KO}$ mice (n=6 for each group). **E** The in vitro experimental schematic for gene validation in isolated splenic NK cells from $Tcf7^{WT}$ or $Tcf7^{KO}$ mice. **F** *Hsp90aa1* mRNA expression in isolated spleen NK cells from $Tcf7^{WT}$ or $Tcf7^{KO}$ mice after hypoxia exposure or under normoxic condition for 24 h (n=3 mice/group for one experiment, repeat 3 experiments). **G** *Hsp90ab1* mRNA expression in isolated spleen NK cells from $Tcf7^{WT}$ or $Tcf7^{KO}$ mice after hypoxia exposure or under normoxic condition for 24 h (n=3 mice/group for one experiment, repeat 3 experiments). **H** Proportion of $Hsp90^+$ NK cells among all NK cells from $Tcf7^{WT}$ or $Tcf7^{KO}$ mice after hypoxia exposure or under normoxic condition for 24 h (n=4/group for one experiment, repeat 2 experiments). **I** Quantification of Hsp90 expression in lung NK cells from $Tcf7^{WT}$ or $Tcf7^{KO}$ mice at day 28 after hypoxia challenge or in ambient air (n=4 for each group). Data represent mean ± SEM. * $P < 0.05$, *** $P < 0.001$, **** $P < 0.0001$ compared to corresponding controls, as analyzed by as analyzed by One-way ANOVA

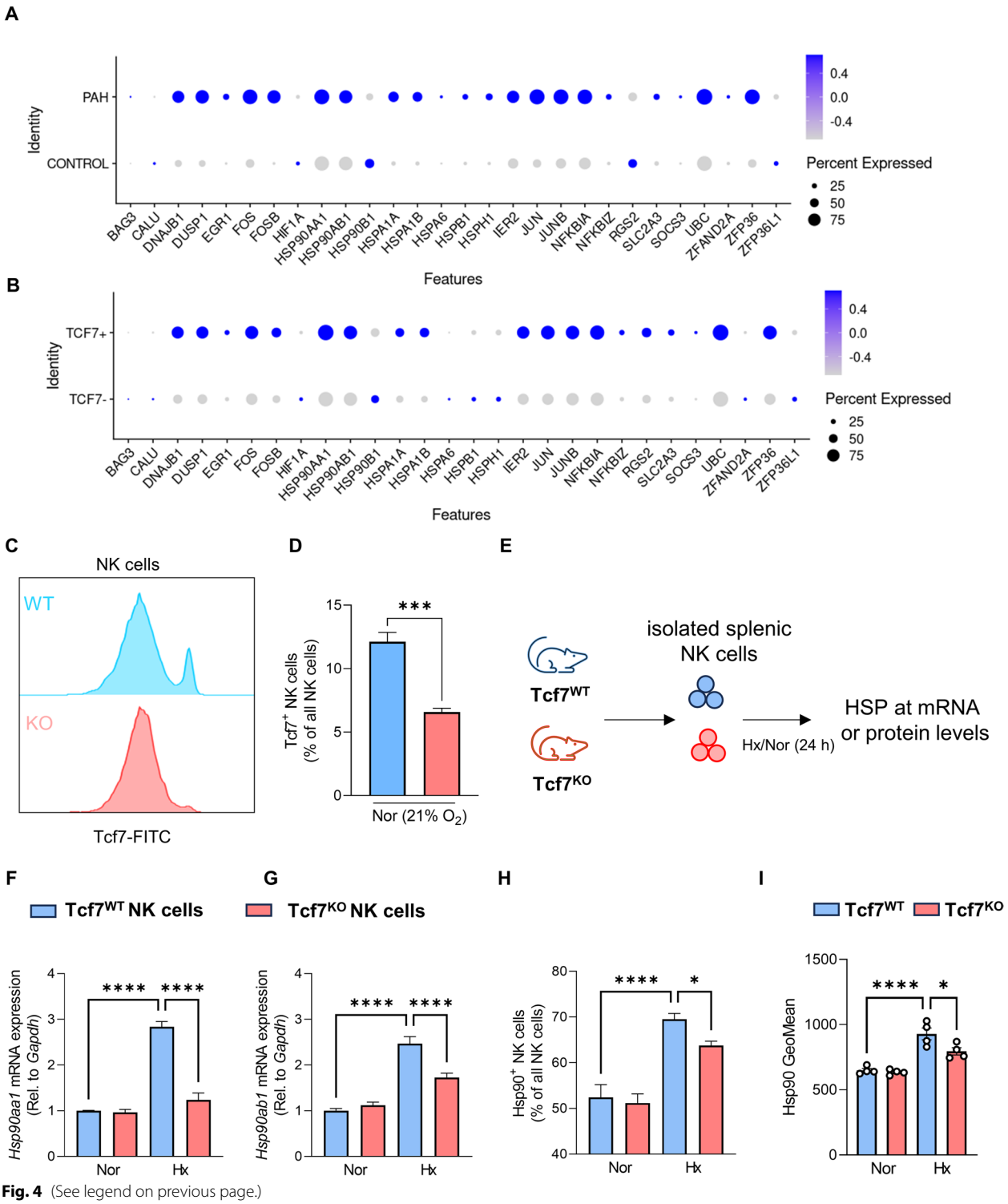

Fig. 4 (See legend on previous page.)

TCF7, a transcription factor well-known for its role in T cell differentiation. In breast cancer, TCF7 expression is principally observed in undifferentiated T cells and is associated with T cell expansion [27]. In cholangiocarcinoma, TCF7 primarily contributes to resistance against the chemotherapeutic agent gemcitabine by upregulating SOX9 expression in cancer cells [28]. In addition, TCF7 appears to extend its regulatory

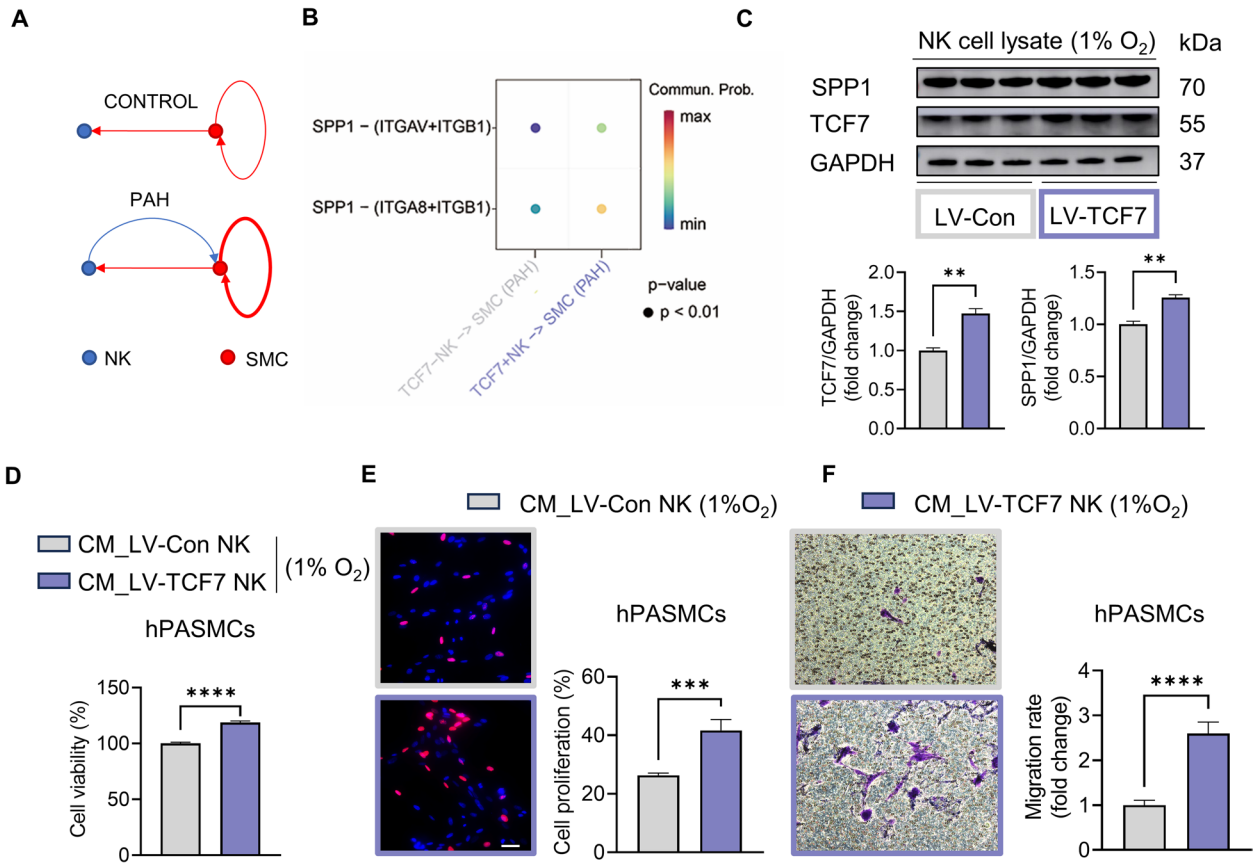

Fig. 5 TCF7 promotes proliferation and migration of PASMCs via upregulating secretion of SPP1 by NK cells. **A** The crosstalk between NK cells and SMCs in lung tissues of human samples from dataset GSE228644. **B** The ligand-receptor pairs in TCF7-deficient NK cells/SMCs and TCF7-expressing NK cells/SMCs. Communication probability refers to the likelihood of specific ligand-receptor interactions occurring between cell types. Red dots represent higher communication probabilities (stronger interactions); blue dots represent lower probabilities (weaker interactions). **C** SPP1 and TCF7 protein expression in LV-TCF7 or LV-Control infected NK92 cells after 48 h hypoxia exposure (n=3/group for one experiment, repeat 2 experiments). **D** The cell viability of hPASMCs after treatment with conditioned medium (CM) from NK92 cells infected with either LV-TCF7 or LV-Control along with 48 h hypoxia exposure (n=6/group for one experiment, repeat 4 experiments). **E** The representative images and quantification of the cell proliferation ability of hPASMCs after treatment with CM from NK92 cells infected with either LV-TCF7 or LV-Control along with 48 h hypoxia exposure (n=3/group for one experiment, repeat 3 experiments). **F** The representative images and quantification of relative migration rate of hPASMCs after treatment with CM from NK92 cells infected with either LV-TCF7 or LV-Control along with 48 h hypoxia exposure (n=3/group for one experiment, repeat 3 experiments). Data represent mean ± SEM. ** $P < 0.01$, *** $P < 0.001$, **** $P < 0.0001$ compared to corresponding controls, as analyzed by unpaired t test. LV-TCF7: Lentivirus carrying TCF7 gene sequence. LV-Con: Lentivirus carrying empty vector

(See figure on next page.)

Fig. 6 TCF7 overexpression aggravates vascular remodeling in MCT-PH rat model. **A** An overview of the experimental design. **B** RVSP (n_1=6, n_2=6, n_3=8, n_4=9); (**C**) mPAP (n_1=6, n_2=6, n_3=7, n_4=6) and (**D**) Fulton index (n_1=6, n_2=6, n_3=9, n_4=11) from AAV6-hTCF7 treated or AAV6-Control rats at day 21 after MCT administration (60 mg/kg) or saline injection. **E** Representative images of EVG staining and (**F**) quantification of media thickness from AAV6-hTCF7 or AAV6-Control recipients at day 21 after MCT or saline injection (n_1=6, n_2=6, n_3=9, n_4=11); scale bar: 50 μm. **G** Representative image of Masson staining and (**H**) quantification of collagen abundance from AAV6-hTCF7 or AAV6-Control recipients at day 21 after MCT or saline injection (n_1=5, n_2=5, n_3=9, n_4=11); scale bar: 50 μm. **I** Representative images of double immunofluorescent staining and (**J**) quantification of α-SMA (for smooth muscle cells) and vWF (for endothelial cells) in lung tissues from AAV6-hTCF7 or AAV6-Control recipients at day 21 after MCT or saline injection (n_1=6, n_2=6, n_3=10, n_4=12); scale bar: 50 μm. **K** Representative images of multiplex immunofluorescent staining assays and (**L**) quantification of the proportion of Hsp90+NK cells among all NK cells in lung tissues from AAV6-hTCF7 or AAV6-Control recipients at day 21 after MCT or saline injection (n_1=5, n_2=5, n_3=5, n_4=5); scale bar: 20 μm. **M** Representative images of western blot and (**N**, **O**) quantification of the protein level of TCF7 and SPP1 in lung tissues from AAV6-hTCF7 or AAV6-Control recipients at day 21 after MCT injection (n_3=5, n_4=5). Data represent mean ± SEM. * $P < 0.05$, ** $P < 0.01$, *** $P < 0.001$ compared to indicated group, as analyzed by One-way ANOVA or unpaired t test. n_1, n_2, n_3 and n_4 denotes the number of rats in group Con-AAV6-Ctrl, Con-AAV6-hTCF7, MCT-AAV6-Ctrl and MCT-AAV6-hTCF7, respectively

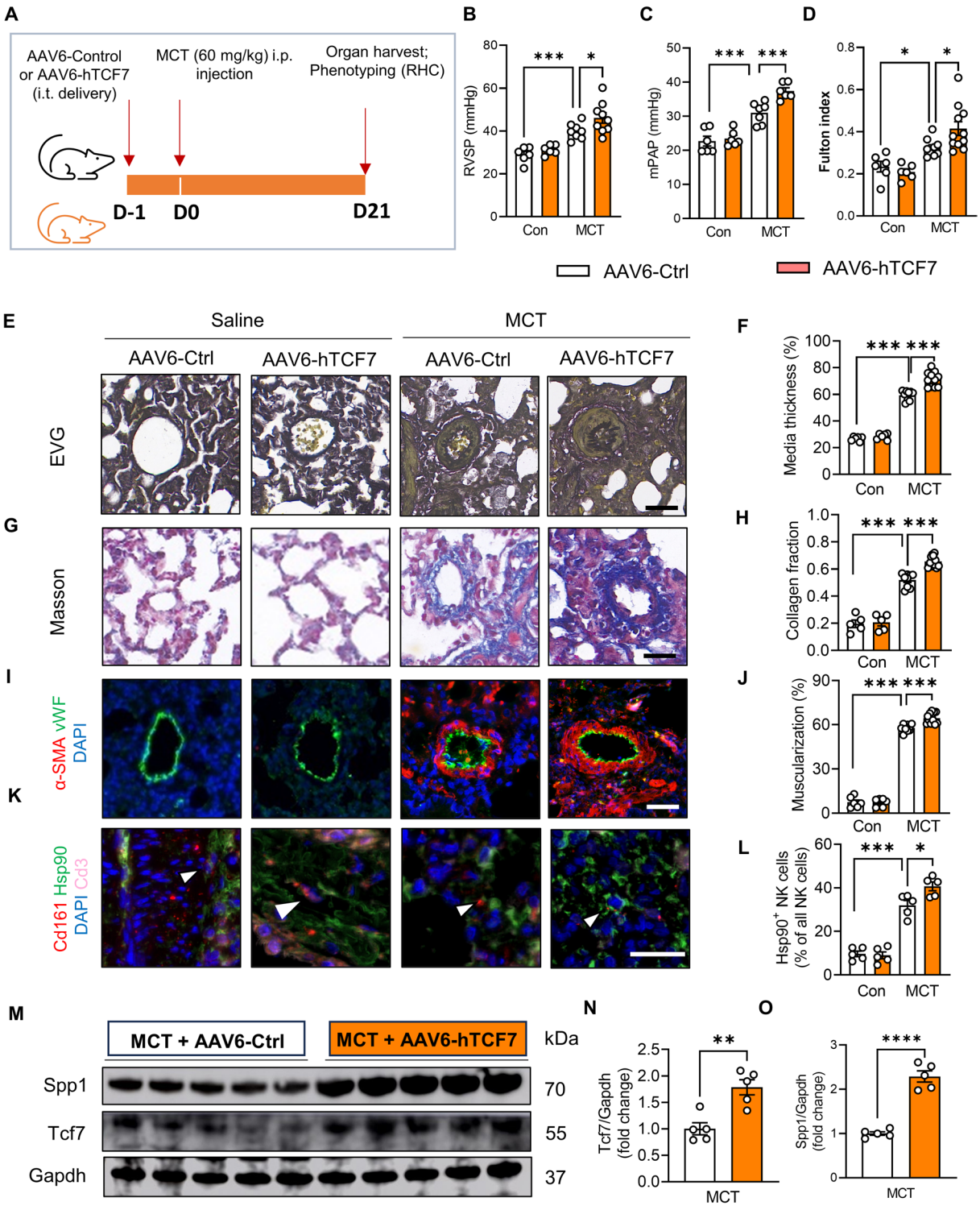

Fig. 6 (See legend on previous page.)

capabilities to innate immune cells [14]. It was reported TCF7 could induce the production of amphiregulin (AREG) by NK cells, which is crucial for the maintenance of NK cell homeostasis and is predominantly suppressed in HIV-1-infected individuals, leading to impaired NK cell function [29]. However, the role of TCF7 in PH has

not been thoroughly investigated, especially regarding its potential regulation of vascular remodeling in PH through the modulation of responses in NK cells; to date, no studies have addressed this issue.

Remarkably, the NK cell with high stress score (NK1 and NK2 subsets) showed an increase of TCF7 expression, which seems to be at the heart of NK cell-related responses in PH. In our study, $TCF7^{+}$ NK cells exhibited higher stress scores may reflect the adaptation of NK cells from compromised cytotoxic function to activation of stress response in the pulmonary vascular microenvironment in the context of PH. This relationship might be mechanistically explained by the modulation of stress-responsive pathways, including MAPK, JAK signaling and WNT signaling [30–32].

Furthermore, we have provided novel insights into the potential molecular mechanisms by which TCF7 drives NK cell responses associated with PH. It was surprisingly observed that TCF7-expressing NK cells expressed abundant stress-related genes compared to TCF-deficient NK cells, which may pertain to a TCF7-dependent stress response in NK cells. HSP90 is a marker gene that responds to cellular stress conditions [33]. Our experimental results confirmed that TCF7 can regulate the stress levels of NK cells through the expression levels of HSP90. SPP1 encodes secreted protein (also known as osteopontin (OPN)) that can bind to receptors on various cell surfaces and exert its effects [34]. There are primarily four biological functions of SPP1. First, SPP1 is a protein that is very important in bone formation and remodeling [35]. It affects the adhesion, migration, and survival of osteoblasts and promotes bone mineralization [36]. Second, SPP1 affects cellular processes such as migration, survival, proliferation, and differentiation by binding to integrin receptors on cell surfaces [37]. Third, in the immune system, SPP1 regulates the function of various immune cells, such as T cells and macrophages, participating in inflammatory responses [38]. Lastly, the expression of SPP1 is associated with the aggressiveness and metastatic ability of certain cancers [39, 40]. It may promote tumor progression by influencing the interaction between tumor cells and the surrounding matrix, as well as the cellular signaling within the tumor microenvironment [41]. Macrophages derived SPP1 can bind to integrin receptors on smooth muscle cells, driving their proliferation [42, 43]. Lines of evidence show that SPP1 upregulation also enhances the proliferative and migratory activity of PASMCs, thereby accelerating PH pathogenesis [44, 45]. Similarly, SPP1 is also upregulated in lung cancer, promoting the proliferation and migration of tumor cells [46]. These findings highlight the central role of SPP1 dysregulation in the progression of diverse pulmonary disorders. Furthermore, our research has confirmed that TCF7 can promote the secretion of SPP1 from NK cells, which in turn further promotes the proliferation and migration of PASMCs. This indicates the specific mechanism by which TCF7 is involved in vascular remodeling, and the development of drugs targeting TCF7 may be key in treating pulmonary arterial hypertension.

This study has several limitations. First, we didn't examine the effect of NK cell-specific deletion of TCF7 on vascular remodeling. At this point, we cannot exclude the possibility that effects of TCF7 on other cells in response to stress differentially or synergistically affect PH in a systemic knockout. Secondly, we didn't provide the direct evidence on how TCF7 regulates the release of SPP1. Future studies are warranted to further elucidate the pathways by which TCF7 influences NK cell activity and how this relates to PH progression. Finally, TCF7, as a transcription factor, plays an important biological role, and therapeutic strategies targeting TCF7 may have off-target effects, underscoring the need for the safety assessments in future preclinical experiments and clinical trials.

(See figure on next page.)

Fig. 7 Tcf7 knockout alleviates vascular remodeling in hypoxia-induced PH mouse model. **A** An overview of the experimental design. **B** RVSP (n_1=7, n_2=5, n_3=7, n_4=9) and (**C**) Fulton index (n_1=8, n_2=9, n_3=7, n_4=7) from $Tcf7^{WT}$ or $Tcf7^{KO}$ mice at day 28 after hypoxia or normoxia. **D** Representative images of EVG staining and (**E**) quantification of media thickness from $Tcf7^{WT}$ or $Tcf7^{KO}$ mice at day 28 after hypoxia or normoxia (n_1=7, n_2=7, n_3=9, n_4=9); scale bar: 50 μm. **F** Representative image of Masson staining and (**G**) quantification of collagen abundance from $Tcf7^{WT}$ or $Tcf7^{KO}$ mice at day 28 after hypoxia or normoxia (n_1=7, n_2=7, n_3=9, n_4=9); scale bar: 50 μm. **H** Representative images of double immunofluorescent staining and (**I**) quantification of α-SMA (for smooth muscle cells) and vWF (for endothelial cells) in lung tissues from $Tcf7^{WT}$ or $Tcf7^{KO}$ mice at day 28 after hypoxia or normoxia (n_1=7, n_2=7, n_3=9, n_4=9); scale bar: 50 μm. **J** Representative images of multiplex immunofluorescent staining assays and (**K**) quantification of the proportion of Hsp90+NK cells among all NK cells in lung tissues from $Tcf7^{WT}$ or $Tcf7^{KO}$ mice at day 28 after hypoxia or normoxia (n_1=5, n_2=5, n_3=5, n_4=5); scale bar: 20 μm. **L** Representative images of western blot and (M, N) quantification of the protein level of TCF7 and SPP1 in lung tissues from $Tcf7^{WT}$ or $Tcf7^{KO}$ mice at day 28 after hypoxia (n_3=5, n_4=5). Data represent mean ± SEM. * $P < 0.05$, ** $P < 0.01$, *** $P < 0.001$, **** $P < 0.0001$ compared to indicated group, as analyzed by One-way ANOVA or unpaired *t* test. n_1, n_2, n_3 and n_4 denotes the number of mice in group Nor-$Tcf7^{WT}$, Nor-$Tcf7^{KO}$, Hx-$Tcf7^{WT}$ and Hx-$Tcf7^{KO}$, respectively

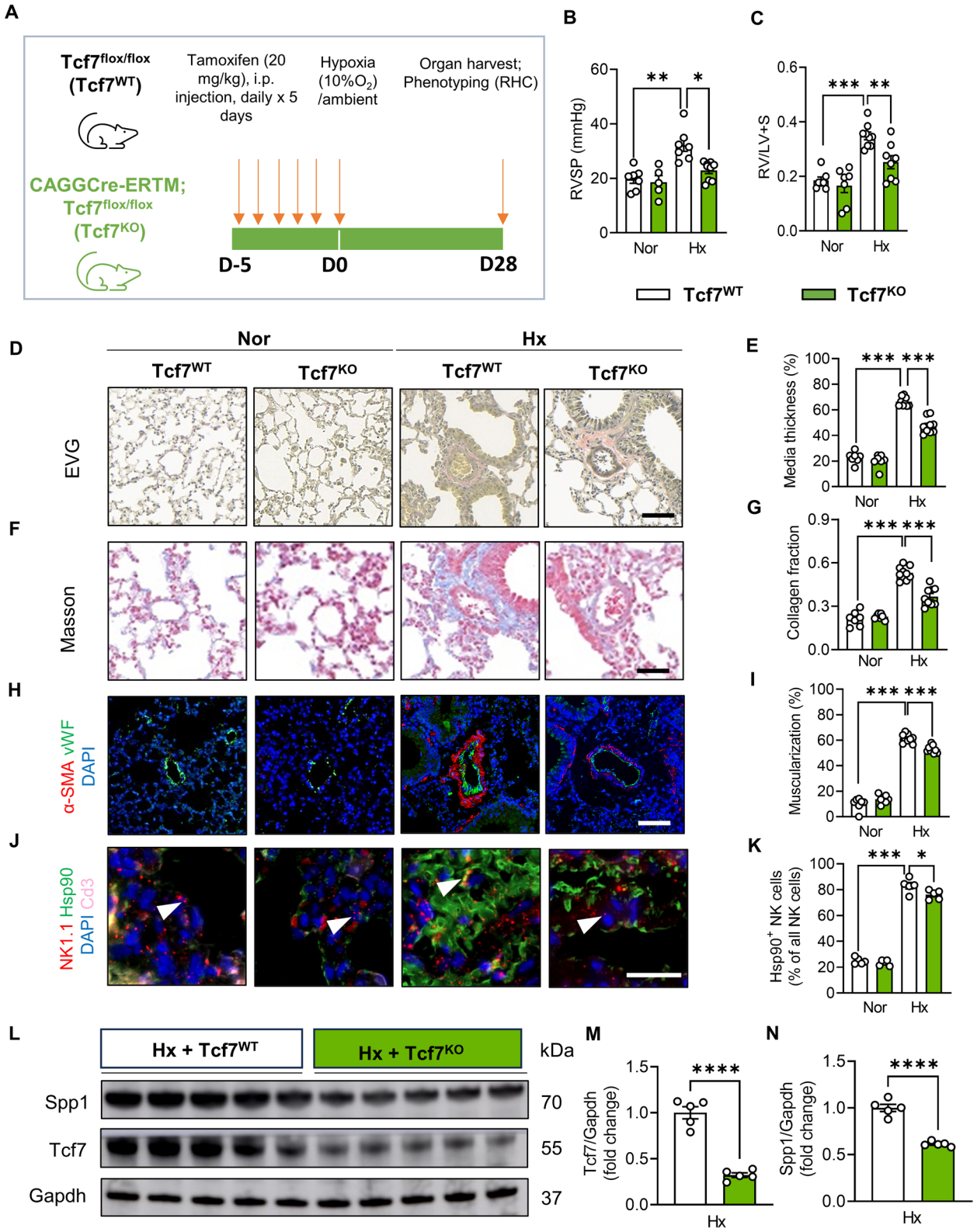

Fig. 7 (See legend on previous page.)

In conclusion, TCF7 emerges as a critical element influencing NK cell behavior and vascular remodeling in PH. Understanding these relationships paves the road for novel therapeutic modalities aimed at the amelioration of PH via the orchestration of immune cell function.

Supplementary Information

The online version contains supplementary material available at https://doi.org/10.1186/s12931-025-03276-9.

Supplementary Material 1.

Supplementary Material 2.

Acknowledgements
Not applicable.

Authors' contributions
Li-Wei Wu, Min Chen and Dai-Ji Jiang carried out animal experiment, contributed to data acquisition, analysis and drafted the manuscript. Chen-Yu Jiang carried out animal experiment and histological staining. Yi-Wei Liu and Bei Feng contributed to data interpretation and manuscript revision. Chen-fei Shi performed RT-PCR for gene validation and flow cytometry. Xu Huang, Xu Zhang and Xiao-He Xu contributed to organ harvest and western blot. Xing-Liang Zhou, Yi Shen and Tian-Yu Liu contributed to data interpretation. Lin-Cai Ye contributed to data interpretation and provided crucial intellectual support. Yang-Yang He, Hao Zhang and Yi Yan conceived and supervised the study and revised the manuscript.

Funding
This work was supported by Shanghai Pujiang Program (22PJ1410100), the Project of National Natural Science Foundation of China (82200065, U20 A2018), Shanghai Key Research Center Construction Project-Shanghai Research Center for Pediatric Cardiovascular Diseases (2023ZZ02024), Young Talent Program of Shanghai Municipal Health Commission (2022YQ070), the National Key Research and Development Program of China (2022YFC2703102), National Clinical Key Specialty Construction Project (10000015Z155080000004), Projects of National Natural Science Foundation of China (82170058, 82241007), Innovative Research Team of High-Level Local Universities in Shanghai, Joint Fund for Science and Technology R&D Plan of Henan Province (222103810055, 232103810056) and Special Project for Key R&D and Promotion of Henan Province (242102311034).

Data availability
All sequencing data in this study were obtained from the GEO (GSE228644) and UCSC databases.

Declarations

Ethics approval and consent to participate
This study has been approved by the Ethics Committee of Shanghai Children's Medical Center affiliated to Shanghai Jiao Tong University School of Medicine (SCMCIRB-K2024081-1), and informed consent has been obtained from the patients or their relative guardians.

Consent for publication
Not applicable.

Competing interests
The authors declare no competing interests.

Author details
[1]Heart Center and Shanghai Institute of Pediatric Congenital Heart Disease, Shanghai Children's Medical Center, National Children's Medical Center, Shanghai Jiao Tong University School of Medicine, Shanghai, China. [2]Shanghai Clinical Research Center for Rare Pediatric Diseases, Shanghai Children's Medical Center, National Children's Medical Center, Shanghai Jiao Tong University School of Medicine, Shanghai, China. [3]Shanghai Research Center for Pediatric Cardiovascular Diseases, Shanghai Children's Medical Center, National Children's Medical Center, Shanghai Jiao Tong University School of Medicine, Shanghai, China. [4]Children's Heart Center, Institute of Cardiovascular Development and Translational Medicine, The Second Affiliated Hospital and Yuying Children's Hospital, Wenzhou Medical University, Wenzhou, China. [5]North Sichuan Medical College, Nanchong, China. [6]School of Pharmacy, Henan University, Kaifeng, China.

Received: 15 September 2024 Accepted: 15 May 2025
Published online: 29 May 2025

References

1. Olsson KM, Corte TJ, Kamp JC, Montani D, Nathan SD, Neubert L, Price LC, Kiely DG. Pulmonary hypertension associated with lung disease: new insights into pathomechanisms, diagnosis, and management. Lancet Respir Med. 2023;11:820–35.
2. Johnson S, Sommer N, Cox-Flaherty K, Weissmann N, Ventetuolo CE, Maron BA. Pulmonary hypertension: a contemporary review. Am J Respir Crit Care Med. 2023;208:528–48.
3. He YY, Yan Y, Jiang X, Zhao JH, Wang Z, Wu T, Wang Y, Guo SS, Ye J, Lian TY, et al. Spermine promotes pulmonary vascular remodelling and its synthase is a therapeutic target for pulmonary arterial hypertension. Eur Respir J. 2020;56:2000522.
4. Shen H, Gao Y, Ge D, Tan M, Yin Q, Wei TW, He F, Lee TY, Li Z, Chen Y, et al. BRCC3 regulation of ALK2 in vascular smooth muscle cells: implication in pulmonary hypertension. Circulation. 2024;150:132–50.
5. Yan Y, He YY, Jiang X, Wang Y, Chen JW, Zhao JH, Ye J, Lian TY, Zhang X, Zhang RJ, et al. DNA methyltransferase 3B deficiency unveils a new pathological mechanism of pulmonary hypertension. Sci Adv. 2020;6:eaba2470.
6. Liu Y, Zhu Y, Jiang C, Su Z, Yan Y, Feng B, Mao W, Zhang Y, Wang X, Xu Z, Zhang H. An electrochemical nitric oxide generator for in-home inhalation therapy in pulmonary artery hypertension. BMC Med. 2022;20:481.
7. Hilton LR, Ratsep MT, VandenBroek MM, Jafri S, Laverty KJ, Mitchell M, Theilmann AL, Smart JA, Hawke LG, Moore SD, et al. Impaired Interleukin-15 signaling via BMPR2 loss drives natural killer cell deficiency and pulmonary hypertension. Hypertension. 2022;79:2493–504.
8. Lepper PM, Bals R, Wilkens H. Natural killer cells in pulmonary arterial hypertension: a force on the dim or the bright side? Circulation. 2012;126:1020–2.
9. Wu SY, Fu T, Jiang YZ, Shao ZM. Natural killer cells in cancer biology and therapy. Mol Cancer. 2020;19:120.
10. Tang F, Li J, Qi L, Liu D, Bo Y, Qin S, Miao Y, Yu K, Hou W, Li J, et al. A pan-cancer single-cell panorama of human natural killer cells. Cell. 2023;186(4235–4251):e4220.
11. Mocumbi A, Humbert M, Saxena A, Jing ZC, Sliwa K, Thienemann F, Archer SL, Stewart S. Pulmonary hypertension. Nat Rev Dis Primers. 2024;10:1.
12. Pais Ferreira D, Silva JG, Wyss T, Fuertes Marraco SA, Scarpellino L, Charmoy M, Maas R, Siddiqui I, Tang L, Joyce JA, et al. Central memory CD8(+) T cells derive from stem-like Tcf7(hi) effector cells in the absence of cytotoxic differentiation. Immunity. 2020;53(985–1000):e1011.
13. Zhang J, Lyu T, Cao Y, Feng H. Role of TCF-1 in differentiation, exhaustion, and memory of CD8(+) T cells: a review. FASEB J. 2021;35:e21549.
14. De Obaldia ME, Bhandoola A. Transcriptional regulation of innate and adaptive lymphocyte lineages. Annu Rev Immunol. 2015;33:607–42.
15. Lauener M, AzadPour S, Abdossamadi S, Parthasarathy V, Ng B, Ostroumov E, Cuvelier GDE, Levings MK, MacDonald KN, Kariminia A, Schultz KR. CD56bright CD16- natural killer cells as an important regulatory mechanism in chronic graft-versus-host disease. Haematologica. 2023;108:761–71.
16. Wang Y, Lifshitz L, Gellatly K, Vinton CL, Busman-Sahay K, McCauley S, Vangala P, Kim K, Derr A, Jaiswal S, et al. HIV-1-induced cytokines deplete homeostatic innate lymphoid cells and expand TCF7-dependent memory NK cells. Nat Immunol. 2020;21:274–86.

17. Jiang Z, Qin L, Tang Y, Liao R, Shi J, He B, Li S, Zheng D, Cui Y, Wu Q, et al. Human induced-T-to-natural killer cells have potent anti-tumour activities. Biomark Res. 2022;10:13.
18. Liu J, Wang Z, Hao S, Wang F, Yao Y, Zhang Y, Zhao Y, Guo W, Yu G, Ma X, et al. Tcf1 sustains the expression of multiple regulators in promoting early natural killer cell development. Front Immunol. 2021;12:791220.
19. Crnkovic S, Valzano F, Fliesser E, Gindlhuber J, ThekkekaraPuthenparampil H, Basil M, Morley MP, Katzen J, Gschwandtner E, Klepetko W, et al. Single-cell transcriptomics reveals skewed cellular communication and phenotypic shift in pulmonary artery remodeling. JCI Insight. 2022;7:e153471.
20. Hao Y, Stuart T, Kowalski MH, Choudhary S, Hoffman P, Hartman A, Srivastava A, Molla G, Madad S, Fernandez-Granda C, Satija R. Dictionary learning for integrative, multimodal and scalable single-cell analysis. Nat Biotechnol. 2024;42:293–304.
21. Hu C, Li T, Xu Y, Zhang X, Li F, Bai J, Chen J, Jiang W, Yang K, Ou Q, et al. CellMarker 2.0: an updated database of manually curated cell markers in human/mouse and web tools based on scRNA-seq data. Nucleic Acids Res. 2023;51:D870–6.
22. Hong J, Arneson D, Umar S, Ruffenach G, Cunningham CM, Ahn IS, Diamante G, Bhetraratana M, Park JF, Said E, et al. Single-cell study of two rat models of pulmonary arterial hypertension reveals connections to human pathobiology and drug repositioning. Am J Respir Crit Care Med. 2021;203:1006–22.
23. Zhou Y, Zhou B, Pache L, Chang M, Khodabakhshi AH, Tanaseichuk O, Benner C, Chanda SK. Metascape provides a biologist-oriented resource for the analysis of systems-level datasets. Nat Commun. 2019;10:1523.
24. MacArthur Clark JA, Sun D. Guidelines for the ethical review of laboratory animal welfare People's Republic of China National Standard GB/T 35892–2018 [Issued 6 February 2018 Effective from 1 September 2018]. Anim Model Exp Med. 2020;3:103–13.
25. Vivier E, Rebuffet L, Narni-Mancinelli E, Cornen S, Igarashi RY, Fantin VR. Natural killer cell therapies. Nature. 2024;626:727–36.
26. Renken S, Nakajima T, Magalhaes I, Mattsson J, Lundqvist A, Arner ESJ, Kiessling R, Wickstrom SL. Targeting of Nrf2 improves antitumoral responses by human NK cells, TIL and CAR T cells during oxidative stress. J Immunother Cancer. 2022;10:e004458.
27. Bassez A, Vos H, Van Dyck L, Floris G, Arijs I, Desmedt C, Boeckx B, Vanden Bempt M, Nevelsteen I, Lambein K, et al. A single-cell map of intratumoral changes during anti-PD1 treatment of patients with breast cancer. Nat Med. 2021;27:820–32.
28. Liu Z, Liu J, Chen T, Wang Y, Shi A, Li K, Li X, Qiu B, Zheng L, Zhao L, et al. Wnt-TCF7-SOX9 axis promotes cholangiocarcinoma proliferation and pemigatinib resistance in a FGF7-FGFR2 autocrine pathway. Oncogene. 2022;41:2885–96.
29. Wang Y, Lifshitz L, Silverstein NJ, Mintzer E, Luk K, StLouis P, Brehm MA, Wolfe SA, Deeks SG, Luban J. Transcriptional and chromatin profiling of human blood innate lymphoid cell subsets sheds light on HIV-1 pathogenesis. EMBO J. 2023;42:e114153.
30. Zhu H, Blum RH, Bernareggi D, Ask EH, Wu Z, Hoel HJ, Meng Z, Wu C, Guan KL, Malmberg KJ, Kaufman DS. Metabolic reprograming via deletion of CISH in human iPSC-derived NK Cells promotes in vivo persistence and enhances anti-tumor activity. Cell Stem Cell. 2020;27(224–237):e226.
31. Song H, Song J, Cheng M, Zheng M, Wang T, Tian S, Flavell RA, Zhu S, Li HB, Ding C, et al. METTL3-mediated m(6)A RNA methylation promotes the anti-tumour immunity of natural killer cells. Nat Commun. 2021;12:5522.
32. Feng C, Yu A, Wang Z, Wang K, Chen J, Wu Y, Deng T, Chen H, Hou Y, Ma S, et al. A novel PDPN antagonist peptide CY12-RP2 inhibits melanoma growth via Wnt/beta-catenin and modulates the immune cells. J Exp Clin Cancer Res. 2024;43:9.
33. Chen B, Piel WH, Gui L, Bruford E, Monteiro A. The HSP90 family of genes in the human genome: insights into their divergence and evolution. Genomics. 2005;86:627–37.
34. Morse C, Tabib T, Sembrat J, Buschur KL, Bittar HT, Valenzi E, Jiang Y, Kass DJ, Gibson K, Chen W, et al. Proliferating SPP1/MERTK-expressing macrophages in idiopathic pulmonary fibrosis. Eur Respir J. 2019;54:1802441.
35. Kruger TE, Miller AH, Godwin AK, Wang J. Bone sialoprotein and osteopontin in bone metastasis of osteotropic cancers. Crit Rev Oncol Hematol. 2014;89:330–41.
36. Foster BL, Ao M, Salmon CR, Chavez MB, Kolli TN, Tran AB, Chu EY, Kantovitz KR, Yadav M, Narisawa S, et al. Osteopontin regulates dentin and alveolar bone development and mineralization. Bone. 2018;107:196–207.
37. Lopes KP, Yu L, Shen X, Qiu Y, Tasaki S, Iatrou A, Beeri MS, Seyfried NT, Menon V, Wang Y, et al. Associations of cortical SPP1 and ITGAX with cognition and common neuropathologies in older adults. Alzheimers Dement. 2024;20:525–37.
38. Argandona Lopez C, Brown AM. Microglial- neuronal crosstalk in chronic viral infection through mTOR, SPP1/OPN and inflammasome pathway signaling. Front Immunol. 2024;15:1368465.
39. Eun JW, Yoon JH, Ahn HR, Kim S, Kim YB, Lim SB, Park W, Kang TW, Baek GO, Yoon MG, et al. Cancer-associated fibroblast-derived secreted phosphoprotein 1 contributes to resistance of hepatocellular carcinoma to sorafenib and lenvatinib. Cancer Commun (Lond). 2023;43:455–79.
40. Yang Y, Jin X, Xie Y, Ning C, Ai Y, Wei H, Xu X, Ge X, Yi T, Huang Q, et al. The CEBPB(+) glioblastoma subcluster specifically drives the formation of M2 tumor-associated macrophages to promote malignancy growth. Theranostics. 2024;14:4107–26.
41. Qi J, Sun H, Zhang Y, Wang Z, Xun Z, Li Z, Ding X, Bao R, Hong L, Jia W, et al. Single-cell and spatial analysis reveal interaction of FAP(+) fibroblasts and SPP1(+) macrophages in colorectal cancer. Nat Commun. 2022;13:1742.
42. Chaulet H, Desgranges C, Renault MA, Dupuch F, Ezan G, Peiretti F, Loirand G, Pacaud P, Gadeau AP. Extracellular nucleotides induce arterial smooth muscle cell migration via osteopontin. Circ Res. 2001;89:772–8.
43. Baron JH, Moiseeva EP, de Bono DP, Abrams KR, Gershlick AH. Inhibition of vascular smooth muscle cell adhesion and migration by c7E3 Fab (abciximab): a possible mechanism for influencing restenosis. Cardiovasc Res. 2000;48:464–72.
44. Meng L, Liu X, Teng X, Gu H, Yuan W, Meng J, Li J, Zheng Z, Wei Y, Hu S. Osteopontin plays important roles in pulmonary arterial hypertension induced by systemic-to-pulmonary shunt. FASEB J. 2019;33:7236–51.
45. Gao RJ, Aikeremu N, Cao N, Chen C, Ma KT, Li L, Zhang AM, Si JQ. Quercetin regulates pulmonary vascular remodeling in pulmonary hypertension by downregulating TGF-beta1-Smad2/3 pathway. BMC Cardiovasc Disord. 2024;24:535.
46. Matsubara E, Yano H, Pan C, Komohara Y, Fujiwara Y, Zhao S, Shinchi Y, Kurotaki D, Suzuki M. The significance of SPP1 in lung cancers and its impact as a marker for protumor tumor-associated macrophages. Cancers (Basel). 2023;15:2250.

Publisher's Note